Atmos. Chem. Phys. Discuss., 11, 21319–21361, 2011
www.atmos-chem-phys-discuss.net/11/21319/2011/
doi:10.5194/acpd-11-21319-2011

Atmospheric Chemistry and Physics Discussions

Link between local scale BC emissions and large scale atmospheric solar absorption

P. S. Praveen[1], T. Ahmed[1], A. Kar[2], I. H. Rehman[2], and V. Ramanathan[1]

[1]Center for Clouds, Chemistry and Climate, Scripps Institution of Oceanography, University of California, San Diego, 9500 Gilman Drive, MC 0221, La Jolla, CA 92093-0221, USA
[2]The Energy and Resources Institute, Darbari Seth Block, IHC Complex, Lodhi Road, New Delhi, 110003, India

Received: 7 June 2011 – Accepted: 17 July 2011 – Published: 28 July 2011

Correspondence to: V. Ramanathan (vramanathan@ucsd.edu)

Published by Copernicus Publications on behalf of the European Geosciences Union.

Abstract

Project Surya has documented indoor and outdoor concentrations of black carbon (BC) from traditional biomass burning cook stoves in a rural village located in the Indo-Gangetic Plains (IGP) region of N. India from November 2009- September 2010. In this paper, we systematically document the link between local scale aerosol properties and column averaged regional aerosol optical properties and atmospheric radiative forcing. We report observations from the first phase of Project Surya to estimate the source dependent (biomass and fossil fuels) aerosol optical properties from local to regional scale. Data were collected using surface based observations of BC, organic carbon (OC), aerosol light absorption, scattering coefficient at the Surya village (SVI_1) located in IGP region, and satellite and AERONET observations at the regional scale (IGP). The daily mean BC concentrations at SVI_1 showed the large increase of BC during the dry season (December to February) with values reaching 35 $\mu g\,m^{-3}$. Space based LIDAR data reveal how the biomass smoke is trapped within the first kilometre during the dry season and its extension to above 5 km during the pre-monsoon season. As a result during the dry season, the variance in the daily mean SSA and column aerosol optical properties at the local IGP site correlated (with slopes in the range of 0.85 to 1.06 and R^2 >0.4) well with the "IGP_AERONET" (mean of six AERONET sites), thus suggesting in-situ observations at few locations can be used to infer spatial mean forcing. The atmospheric forcing due to BC and OC exceeded 20 $W\,m^{-2}$ during all months from November to May, leading to the deduction that elimination of cook stove smoke emissions through clean cooking technologies will likely have a major positive impact on health and the regional climate.

ACPD

11, 21319–21361, 2011

1 Introduction

Roughly half of the world's population relies on solid fuels (wood, animal dung, crop residues and coal) for daily household energy needs. Cooking with these fuels emits significant amount of smoke (comprising mainly of soot and semi-volatile organics) due to incomplete combustion. For most part, cooking is done in the kitchen microenvironment with poor ventilation causing extensive build-up of smoke; resulting in the exposure to high levels of particulate matter which causes adverse health effects (Sauvain et al., 2006; Smith et al., 2004; Schwarze et al., 2006). This indoor smoke escapes outdoors and leads to atmospheric brown clouds (ABCs) (Ramanathan et al., 2001a).

Black carbon (BC), a major component of smoke, strongly absorbs sunlight in the atmosphere and is considered to be the second largest contributor to global warming after CO_2 (Ramanathan and Carmichael, 2008; Jacobson, 2010). BC significantly impacts the regional and global climate through the disruption of monsoon, retreat of glaciers, arctic sea ice and mountain glaciers (Ramanathan et al., 2001a; Lau et al., 2008; Menon et al., 2002, 2010; Flanner et al., 2009; Pettus, 2009). Because of its positive atmospheric radiative forcing (i.e., warming) and relatively short residence time in the atmosphere (few days to weeks) compared to CO_2 (lifetime of more than 100 yr), reducing BC emissions presents unique opportunities for delaying the impacts of climate change (Ramanathan and Wallack, 2008; Molina et al., 2009; Ramanathan and Xu, 2010). Organic carbon (OC), co-emitted along with BC, was previously known to have negligible solar absorption and thus assumed to have only a cooling effect (Andreae and Gelencser, 2006). However, studies have shown that some OC fractions (referred to as brown carbon) emitted mostly during biomass burning show strong wavelength dependence of absorption in the ultraviolet and visible region (<600 nm) (Kirchstetter et al., 2004), thus adding to positive atmospheric radiative forcing.

Biofuel combustion is the predominant source of BC over Africa (72 %) and South Asia (68 %) (Reddy and Boucher, 2007). Over India, BC emissions from fossil fuel, open burning, and biofuel combustion contributes around 25 %, 33 %, and 42 %, re-

ACPD
11, 21319–21361, 2011

spectively (Venkatraman et al., 2005). Model simulation has shown that replacing traditional methods of cooking (i.e., burning biomass fuel in mud stove) with improved cook stoves may significantly reduce atmospheric BC burden over South and East Asia (Ramanathan and Carmichael, 2008). The Indo-Gangetic Plains (IGP), situated along the southern edge of the Himalayan region and spanning across the north-eastern parts of India, is one of the most densely populated regions on earth. It is characterized by large anthropogenic emissions that include biofuel emissions from rural households, thermal power plants and industries, causing a widespread layer of ABCs over the region (Ramanathan and Ramana, 2005). MODIS aerosol optical depth indicates that the IGP region is subjected to a heavy loading of the pollution layer (Fig. 1). *Project Surya* is the first field study designed to demonstrate the potential of mitigating biomass BC emissions on slowing down global warming and reducing negative health effects (Ramanathan and Balakrishnan, 2007). The first (or pilot) phase of Project Surya was started in October 2009 in a rural village located in the IGP region in northern India. The first phase observations were devoted to baseline measurements of BC concentration and aerosol optical properties from both indoor and outdoor.

This is the third in a series of 4 papers on the first phase study. The first paper (Ramanathan et al., 2011) deals with a cell-phone based BC monitoring system for large scale (e.g. 100–300 households) measurements. The second paper (Rehman et al, 2011) explored the link between indoor and outdoor BC concentration. The fourth paper (Kar et al., 2011) investigates different commercially available improved cook stoves in cutting down BC emissions. This study documents the baseline BC measurements on diurnal, daily and seasonal time scales and examines the source dependent aerosol light absorption characteristics. As one of the main goals of Project Surya is to document the impact of BC mitigation on regional climate, this study also integrates the surface data collected in the village with other ground-based network and satellite observations to probe the link between local-scale emissions and regional-scale atmospheric BC solar absorption.

ACPD
11, 21319–21361, 2011

2 Experimental

2.1 Site description

Project Surya's observational campaign was started on 15 October 2009 in a typical Indian rural village (26° N, 81° E) located in the IGP region (Fig. 1). The Surya village (denoted as SVI_1 from hereafter) is nearly 3 km away from a national highway, about 2 km from a state highway, and is located within 15 km radius of an industrial zone. The SVI_1 has around 485 households in seven close by hamlets. We conducted experiments in the largest hamlet that has around 200 households. Most of the households use biomass as cooking fuel. Outdoor fires (for relief during the cold winter) and occasional open burning of crop residue are the other major sources of biomass originated aerosol apart from cooking. Vehicular and industrial emissions are the fossil fuel sources in the region.

2.2 Instrumentation

Observations were classified as indoor and outdoor measurements. For indoor observations, concentration of real-time BC and integrated elemental carbon (EC) were measured in the kitchen microenvironment in selected SVI_1 households. Real-time BC was measured using a single wavelength (880-nm) microAeth Model AE51 (Magee Scientific, Berkeley, CA). Three AE51 instruments (MA158, MA160, and MA165) were used for indoor BC measurement. The flow rate used for sampling was 50 mlpm with a time base of 1 min. Also 24-h indoor integrated aerosol samples were collected on quartz filter using a novel cell phone based BC monitoring system (BC_CBM). These filter samples were subjected to EC/OC analysis using thermal-optical EC/OC analyzer (Schauer et al., 2003). Details of indoor sampling and analysis using BC_CBM and AE51 were given in Ramanathan et al., (2011) and Rehman et al. (2011).

Outdoor measurements consist of measuring real-time BC concentration and aerosol scattering coefficient to understand the aerosol heating and cooling proper-

ACPD
11, 21319–21361, 2011

ties predominated by biomass aerosols. For this purpose, we chose sampling site at the center of the SVI_1 (denoted as VC site). We also measure BC at the northeast corner of the SVI_1 (denoted as NEV site) to understand aerosol spatial variability in the village. The distance between the NEV and VC sites is approximately 250m. At NEV, real-time BC concentration measurements were started on 15 October 2009 using 7-wavelength Aethalometer Model AE42 (Magee Scientific, Berkeley, CA). At VC, real-time measurement of both BC and aerosol scattering coefficient were started on 1 November 2009; BC was measured using 7-wavelength Aethalometer Model AE31 (Magee Scientific, Berkeley, CA) and aerosol scattering coefficient was measured using single wavelength (550-nm) integrating nephelometer Model M9003 (ECHOTEC). In addition, one-week observations of BC and aerosol scattering coefficient were also conducted at the highway (nearest traffic junction from the SVI_1) during 19–27 November 2009 using AE42 and nephelometer to understand fossil fuel contribution.

Both AE42 and AE31 were operated with a flow rate set at 2 lpm and measurement frequency of 2 min. Nephelometer was operated at a sample flow of 5 lpm. The scattering response of the nephelometer was calibrated using CO_2 as a span gas and filtered air as zeroing gas. Nephelometer has different illumination sensitivity for coarse and fine particles because of truncation of forward scattering; the instrument cannot detect forward scattered light between 0–7 degrees (Anderson and Ogren, 1998). However, we did not use any correction factor to account for angular truncation error of nephelometer data, since illumination function in the ECHOTEC nephelometer deviates significantly from other commercially available nephelometers (Müller et al., 2009). The instruments at both VC and NEV sites were deployed on the roof under the shade. The air sampling inlet was mounted at a height of ~10 m above the ground; stainless steel tubing was used for sample intake. The inlet system was designed to prevent entry of raindrops or insects in the sample stream. BC measurements were tested with and without inlet system to check any particle loss. The slope and correlation coefficient of the comparison between BC measurement with and without inlet system (plot not shown here) were found as 0.99 and $R^2 = 0.78$, respectively, suggesting minimal

ACPD
11, 21319–21361, 2011

particle loss.

2.3 Data processing and validation

AE31 and AE42 aethalometers measures attenuation of the light beam at seven different wavelengths (370, 470, 520, 590, 660, 880 and 950 nm) after transmitted through aerosols that are being continuously deposited on a quartz fiber filter. The aethalometer manufacturer (Magee Scientific) calibrates the instrument based on the assumption that the change in aerosol light attenuation coefficient (m^{-1}) is proportional to BC concentration ($g\,m^{-3}$) through a constant called specific absorption cross section ($m^2\,g^{-1}$). The 880 nm channel is recommended by the manufacturer for BC measurement. However, due to aerosol-filter interactions (such as multiple light scattering effects within the filter and the "shadowing" effect due to filter loading), the aethalometer observed aerosol attenuation coefficient is larger than the actual air-borne aerosol absorption coefficient (Arnott et al., 2005; Schmid et al., 2006). Correction methods are well documented in recent literature to obtain the actual air-borne aerosol absorption coefficient from aethalometer aerosol attenuation coefficient data (Arnott et al., 2005; Schmid et al., 2006). The present data analysis follows the Schmid et al. (2006) method to derive air-borne aerosol light absorption coefficient at seven wavelengths from the aethalometer data. The derived aerosol light absorption coefficient is then converted to BC concentration by dividing with a specific absorption cross section value. A wide range of values have been reported for specific absorption cross section ($2–25\,m^2g^{-1}$) for ambient BC aerosols depending upon the source, location, and age of the aerosol; we used a value of $10\,m^2\,g^{-1}$ for 880-nm channel, the value often found in literature for air-borne BC particle (Schwarz, 2008; Ram and Sarin, 2009). We used the same approach for correcting data from AE51 instruments.

We first checked the response of aethalometer to pure biomass and fossil fuel combustion aerosol. For this purpose AE31 instrument was operated for about an hour near a biomass cook stove and a diesel vehicle exhaust. Figure 2 shows the wavelength dependence of the normalized light absorption coefficient for both the sources.

ACPD
11, 21319–21361, 2011

The spectrally dependent aerosol absorption coefficient is given by a power law relationship $\sigma_\lambda = C\ \lambda^{-AAE}$, where σ_λ is the aerosol absorption coefficient at wavelength (λ), C a constant, and AAE is the absorption Angstrom exponent (Kirchstetter et al., 2004). Biomass aerosol show high absorption in the UV and visible regions compared to fossil fuel aerosol. In the present study AAE of absorption coefficient was calculated by the negative slope of absorption vs. wavelength in a log-log plot (for wavelengths 370 to 950 nm). Our results show that the mean AAE value of biomass was observed as 2.2; while for fossil fuel the value was 1.17. The observed aethalometer response is in close agreement with earlier reported values (Bergstrom et al., 2007; Kirchstetter et al., 2004).

It is essential to check the BC measurement precision among AE31, AE42, and three AE51 aethalometers for the same ambient air sample. Figure 3 shows the individual comparisons among different aethalometers. All three AE51 (MA158, MA160, MA165) were tested for precision in a rural household kitchen environment near a cook stove after connecting parallel to each other with a single inlet. Figure 3a–c shows comparisons among three AE51 instruments. BC measurements from all three AE51 agreed well with each other (slope ranging from 0.9 to 0.97, and correlation coefficient R^2 ranging from 0.98 to 0.99). Figure 3d–f show comparison of BC measurements of co-located aethalometers AE 31, AE42 and AE51 (model MA160). The slope of intercomparison ranged from 0.87 to 0.99 and R^2 ranged from 0.79 to 0.88, indicating good agreement with each other.

Finally we compared the ambient BC measurement from AE31 (used as a representative of aethalometer measurement) at VC with standard EC measurement from thermal-optical method. Figure 4 shows the comparison between aethalometer AE31 measured BC and thermal-optical measured EC in filters collected using BC_CBM system running simultaneously with AE31. The slope and R^2 of the comparison were found as 0.86 and 0.52, which is well within the range observed by many earlier studies. In our results BC is found to be 14 % lower compared to EC. Partly this could be attributed to loss of BC data during frequent aethalometer tape advance, especially

ACPD
11, 21319–21361, 2011

during peak BC concentration. In a typical observation day, 10–15 % BC data was lost due to tape advance.

3 Results

3.1 Daily and monthly variation of BC concentrations in the SVI_1

Figure 5 shows the daily and monthly mean variations of BC concentrations at the VC site from November 2009 to May 2010. Daily mean BC concentration at VC during the study period varied from 3 to 56 $\mu g\,m^{-3}$ with a mean value of 14.6±7.5 $\mu g\,m^{-3}$. BC concentrations were found to be higher during the winter (or dry) season (December to February) compared to the pre-monsoon season (March to May). The highest monthly mean BC concentration at VC was observed in December (22.5±5.2 $\mu g\,m^{-3}$), and after a gradual decrease to a lower value in March (8.7±2.4 $\mu g\,m^{-3}$), the concentrations were found to increase again to 16±3.9 $\mu g\,m^{-3}$ in April. High BC concentrations in winter may be attributed to increase in the intensity of outdoor fires (for relief during the cold winter) and meteorological conditions like low wind speeds and low level inversion. The effects of meteorological conditions are further explained in Sect. 5.1. The rise in ambient BC concentrations in April could be attributed to an increase in open burning activity (Beegum et al., 2009). This is further supported by the fire activity data from MODIS (plot not shown here) which showed that during the study period fire pixel count in the region (29–24° N, 85–75° E) peaked in the month of April, 2010. Venkatraman et al. (2006) also reported that BC emission from forest fires peaked in March and from crop residue burning peaked in May and October in India. The NEV site had a mean ambient BC concentration of 17.4±6.2 $\mu g\,m^{-3}$ during 15 October 2009–30 April 2010. Comparison between BC measured at VC and NEV (plot not shown here) produced slope of 0.96 and R^2 of 0.64 indicating there is not much spatial variation within the village.

ACPD
11, 21319–21361, 2011

3.2 Diurnal variation of BC in the SVI_1

Figure 6 shows the seasonal mean diurnal variation of ambient BC concentration at VC. The diurnal variation of BC in all four seasons showed similar trend; with twice daily maximum in BC concentration in the morning between 06:00 and 09:00 LT and in the evening between 17:00 and 20:00 LT closely coinciding with the morning and evening cooking hours in the village. BC concentrations decreased gradually from morning to noon due to increase convective activity, reaching its minimum value between 12:00 and 15:00 LT. As the night progresses anthropogenic activities are reduced, and as a result peak BC concentration gradually decreases. The morning and evening peak BC concentrations during the monsoon season were very low compared to other seasons (dry, pre-monsoon and post-monsoon).

3.3 Comparison of SVI_1 BC with previous measurements in the region

In the past decade, there have been many observational campaigns and long-term monitoring studies for BC measurements in different parts of India covering urban, rural, costal, marine and high altitude environments (see Table 1). Reported BC concentration over Indian cities were found to be quite high compared to cities in other parts of the world (Ganguly et al., 2006; Latha and Badarinath, 2005; Babu and Moorthy, 2002). The observed BC concentrations in India showed large spatial variations depending on the location (Table 1); with mainland BC concentrations (especially urban centers and IGP region) being much higher than those at high altitude and island stations. Total and BC aerosol concentrations were 5–10 times higher over the IGP region compared with non-IGP locations (Nair et al., 2007; Beegum et al., 2009). The observed daily mean and diurnal variation of BC concentrations at SVI_1 are within the range of reported values in the region (Beegum et al., 2009).

ACPD
11, 21319–21361, 2011

4 Characteristics of solar absorption by BC

4.1 Time series of aerosol scattering and absorption coefficient

Figure 7a shows the daily mean variation of aerosol scattering and absorption coefficient at VC during the study period. Aerosol scattering coefficient showed an increasing trend from the post monsoon season to winter season, and then a decreasing trend from winter towards the monsoon season. Aerosol absorption coefficient followed a similar trend as BC (Fig. 5) but unlike the scattering coefficient trend, it did not have a maximum during winter. The winter time peak in the scattering coefficient coincides with a corresponding peak in the relative humidity (daily mean RH shown in Fig. 7b), thus implying hygroscopic growth of the aerosol (Pan et al., 2009). Layer of non-absorbing coating (such as water vapour) on BC aerosol is also known to enhance its absorption. However, with the increase in the size of aerosol with increasing relative humidity, enhance scattering due to much larger aerosol surface area is likely to offset enhance absorption.

The aerosol single scattering albedo (SSA), which is the ratio of scattering to the extinction coefficient, is one of the important parameters that determine the impact of aerosols on radiative forcing. Figure 7c illustrates the daily mean variation of surface SSA at VC along with columnar SSA (from AERONET) at adjacent urban center Kanpur (26.30′ N, 80.31′ E). Between January and March, VC and Kanpur SSA were in a similar range with values ranging between 0.7 and 0.95. However, in the other months VC SSA values were mostly less than 0.8 compared to Kanpur columnar SSA. When SSA<0.9, aerosol significantly heats the atmosphere and reduces solar radiation at the surface, thus causing large impact on regional climate and the hydrological cycle (Ramanathan et al., 2001a; Krishnan and Ramanathan, 2002; Menon et al., 2002).

Figure 8 shows the diurnal variation of aerosol absorption, scattering coefficient, along with SSA for VC and the highway. The aerosol scattering and RH absorption coefficient showed a similar diurnal pattern at VC and the highway, with slightly higher values observed at highway. SSA values were observed to be high in the afternoon

ACPD
11, 21319–21361, 2011

time between 12:00 and 15:00 LT for both the VC and the highway locations even though the RH was observed very low. During noon time secondary aerosol production through photochemical processes may be enhance light-scattering, which may reflected in high SSA (Yan et al., 2008). Further SSA showed decreasing trend in evening hours and then increased towards night time. The absorbing aerosols (BC) are emitted directly from combustion sources (cook stoves, vehicles), whereas some of the scattering aerosols are formed by gas to particle conversion process (Lyamani et al., 2010). This delay in the formation processes of absorbing and scattering aerosol and an increase in BC emission from cook stoves and vehicles may cause the dip in SSA in the evening hours. Similar processes should also effect morning peak emission hours, however the SSA did not show any dip, and this need further investigation.

4.2 Absorption Angstrom exponent

It has been shown earlier (Kirchstetter et al., 2004) that the spectral dependence of light absorption can be used to distinguish aerosols originating from fossil fuel and biomass fuel combustion. The presence of brown carbon (light absorbing OC mainly from biomass combustion) enhances the aerosol light absorption in the blue and the ultraviolet region (λ<600 nm). Understanding the spectral dependence of aerosols is important in order to properly account for their absorption in radiative transfer models.

Figure 9a and b show the normalized aerosol light absorption of aerosol at highway and the VC during cooking and non-cooking hours. Also shown in the figure are our observed aethalometer response (from Sect. 2.3) to biomass (wood in cookstove) and fossil fuel (diesel) combustion aerosol, along with the previously published (Kirchstetter et al., 2004) observations. Clearly distinct aerosol light absorption pattern can be seen for biomass and fossil fuel sources aerosol. Both published and observed Aethalometer response data indicate that the normalized aerosol light absorption at 370 nm is ~5 times higher compared to the 700 nm for biomass combustion sources and ~2 times higher for fossil fuel combustion sources. Aerosol light absorption falling in between the two extremes of biomass and fossil fuel absorption pattern will be indicative of

ACPD
11, 21319–21361, 2011

mixing of aerosol from the two sources. Normalized aerosol light absorption at both VC (Fig. 9b) and the highway (Fig. 9a) location indicates that the aerosol sources are influenced by both biomass and fossil fuel sources; with VC normalized aerosol light absorption falling closer to pure biomass absorption line, suggesting higher contribution of biomass aerosol. Interestingly, at the highway aerosol light absorption showed enhanced absorption in shorter wavelength during cooking hours compare to non-cooking hours, strongly suggesting influence of biomass cooking activity on highway aerosol. During non-cooking hours the normalized aerosol light absorption at highway was closer to pure fossil fuel absorption line indicating the dominance of fossil fuel (diesel) generated aerosol.

Several studies have found that aerosols originating from fossil fuel combustion show weaker dependence on spectral light absorption, with the absorption Angstrom exponent (AAE) value close to 1 (Bergstrom et al., 2007; Kirchstetter et al., 2004). However for aerosol emitted from biomass burning, the values of the AAE have been reported between 1.5 and 3; a value of 2 often considered as a mean (Bergstrom et al., 2007; Kirchstetter et al., 2004). An AAE value between 1 and 2 could be indicative of aerosol of mixed origin, i.e., fossil and biomass fuel. The mean AAE values for the VC and the highway are found as 1.81 and 1.61, respectively. It is understandable that the lower value was observed at the highway since fossil fuel contribution was higher there compared to other locations. The higher value observed at the VC is due to high contribution of aerosol from biomass combustion sources, as almost all households use biomass as cooking fuel. The AAE values at VC showed a similar diurnal pattern as BC (Fig. 10), with two prominent peaks – one in the morning hours of 06:00–09:00 LT and the other during the evening hours of 17:00–20:00 LT. BC peaks depend on sources and meteorology conditions, whereas the AAE peaks indicate relatively different contributions from sources during that time. Peak values of AAE at VC during cooking hours reached between 2.0 and 2.2, suggesting that biomass contribution was most dominant during this period. The major biomass burning activities during this time were observed to be cooking and winter outdoor fires. The highway AAE showed slight

ACPD
11, 21319–21361, 2011

diurnal variation with values in the range of 1.4–1.7. The highway AAE peaks were not sharp but the values increased slightly during cooking hours, indicating some influence from cooking. However, the AAE range suggests that there was a contribution from biomass sources.

5 Local to regional scale linkages

5.1 Vertical variations and transport of aerosol

The fundamental mechanism for local to regional scale propagation of pollution is to vertically transport (e.g. pumping by cumulus convection) from the surface layer to the free troposphere above, then from there carried by faster winds to other regions. The Cloud-Aerosol Lidar and Infrared Pathfinder Satellite Observation (CALIPSO) satellite provides high-resolution vertical distribution of aerosol and clouds and offers a unique opportunity to study vertical transport of aerosol. The CALIPSO lidar instrument known as CALIOP (Cloud-Aerosol Lidar with Orthogonal Polarization) measures the depolarized aerosol back-scattered light at two wavelengths (532 and 1064 nm). Figure 11 shows the monthly mean CALIOP LIDAR level-2 extinction profiles from the grid (26–27° N and 80–82° E) over the observation location.

During the monsoon season (June - September), air flow in the lower troposphere is predominantly westerly over India, which brings a large influx of moist air from the Arabian Sea. During the post monsoon season (October–November) the westerly flow weakens in the lower troposphere and the easterly flow sets in. From the post-monsoon to the dry (winter) season (December–February), the daily mean surface temperatures gradually decreases, reaching minimum values in the dry season. Fair weather conditions with clear skies and dry conditions exist during the dry season. As shown in Fig. 11 for the post-monsoon season, the aerosols were mostly confined within ~2 km from the surface with maximum seasonal extinction coefficient value of ~0.5 km^{-1} (observed during the month of November at ~0.5 km altitude). Almost no

ACPD
11, 21319–21361, 2011

aerosol layer was observed above ∼3 km during the post-monsoon season. The observed BC concentration at the surface was 13.8±7.6 μg m^{-3} in post monsoon season. During the dry season, low level inversions leads to shallower aerosol layer compared to the pre-monsoon season resulting in accumulation of pollutants near the surface. This is clearly seen in Fig. 11; the extinction coefficient reached its highest values of ∼1.7 km^{-1} at ∼0.5 km altitude during the month of December in the dry season. Also no aerosol layer were observed above ∼2 km in the winter season compared to ∼3 km for post-monsoon season further suggesting suppression of vertical transport of aerosol layer during winter. This is reflected in the surface BC concentration which reaches a maximum (16.3±8.8 μg m^{-3}) in the winter. During the pre-monsoon season (March–May) the weather is very hot and dry, with deep boundary layer and maximum daytime temperature reaching as high as 45 °C. During this season, dust content in the atmosphere is high, as well as open burning activities (forest fires and crop residue burning) are common. The monthly mean extinction profiles indicate that the aerosol layer is transported as high as ∼5 km due to vertical mixing and convection, resulting lower BC concentration (12.7±5 μg m^{-3}) at the surface.

5.2 Regional scale correlations

Aerosol optical depth (AOD) is a measure of the columnar extinction of light due to aerosol and is also measure of the total number of aerosol in the column. The vast IGP region has higher AOD values than the rest of India during all seasons (Ramanathan and Ramana, 2005; Ramana et al., 2004; Chung et al., 2010). MODIS (Moderate-resolution Imaging Spectroradiometer) level-3 AOD data was used to quantify aerosol column content at SVI_1 and regional mean of IGP (denoted as "IGP_MODIS"). The region considered for IGP_MODIS is shown as dashed line in Fig. 1. Figure 12 illustrates the daily variation of AOD at SVI_1 (MODIS) and Kanpur (AERONET). The SVI_1 AOD showed a similar trend with neighbouring (130 km away from SVI_1) urban centre Kanpur. Comparison between SVI_1 AOD and Kanpur AOD (plot not shown here) yielded slope of 0.89 and R^2 of 0.55. Seasonal AOD variations in the IGP region show

ACPD
11, 21319–21361, 2011

two prominent peaks – during the winter (December–January) and the pre-monsoon period (March–May). The winter peak is attributed to biomass burning and anthropogenic activities, whereas the pre-monsoon peak is influenced by dust aerosol from the western Thar Desert (Prasad et al., 2007). Aerosol during winter is found to be of a highly absorbing nature (Tripathi et al., 2005; Ganguly et al., 2009).

The NASA AERONET began a four-year intensive field campaign on April 2008, called TIGERZ, to measure aerosol microphysical and optical properties over India. We considered mean of six TIGERZ AERONET stations (shown in Fig. 1) data in IGP region (denoted as "IGP_AERONET") to study local to regional aerosol propagation, by inter-comparing aerosol column optical properties between Kanpur (local) vs. IGP_AERONET. Errors in AERONET SSA and AAOD were estimated to be high for lower AOD values and dependent on solar zenith angles (Dubovik et al., 2002). For this study, we consider level-1.5 data points as valid for AOD 675 nm >0.2 and solar zenith angle between 45°–75° during November 2009–May 2010.

Figure 13a–f illustrates the comparison between local to regional scale AOD, SSA, AAOD, Angstrom exponent of the AOD (AE), and Angstrom exponent of AAOD (AAE_c). MODIS AOD at SVI_1 was correlated with IGP_MODIS AOD with $R^2 = 0.72$ and slope = 0.97 (Fig. 13a). Similarly, AERONET AOD at Kanpur (local scale) was correlated with IGP_AERONET AOD with $R^2 = 0.62$ and slope = 0.92 (Fig. 13b). We observed similar correlation between local (SVI_1) to IGP_MODIS AOD for individual months (Fig. 14). This indicates that the column aerosol content was symmetrically spread over the region during all seasons. The AE is usually used to describe the spectral dependence of the aerosol optical depth on wavelength. The AE is a useful quantity to assess the particle size of atmospheric aerosol, ranging from 4 for very small particles (AE >1 for fine particle dominance) to 0 for very large particles (AE <1 for coarse particle dominance). In the present study AE was calculated by the negative slope of AOD vs. wavelength in a log-log plot (for wavelengths 437 to 1020 nm). Local scale AE was correlated with IGP_AERONET AE with $R^2 = 0.79$ and slope = 0.89 (Fig. 13c), indicating that particle dominance – either fine or coarse – is identical with

ACPD
11, 21319–21361, 2011

the regional scale. The local scale SSA was correlated with the IGP_AERONET SSA with $R^2 = 0.52$ and slope = 1.01 (Fig. 13d), indicating that the relative contribution of scattering and absorbing aerosol haave a similar fraction at the regional and the local scale. AAE_c is a good indicator of sources of absorbing aerosols. AAE_c is observed to be near 3 for dust aerosols, near 1 for urban and industrial aerosols, and greater than 1 for biomass aerosols (Bergstrom et al., 2007; Russell et al., 2010). In the present study AAE_c was calculated by the negative slope of AAOD vs. wavelength in a log-log plot (for wavelengths 437 to 1020 nm). The local scale AAE_c correlated with IGP_AERONET AAE_c with $R^2 = 0.52$ and slope = 1.06 (Fig. 13f), indicating that local to regional sources of observing aerosols are similar.

The observed AE of the IGP_AERONET was in the range of 0.1–1.6 indicating varying aerosol compositions, including dust domination to fine particles from biomass, urban and industrial sources. Particularly, during April–May 2010, AE was in the range of 0.1–0.8 indicating dust influence, perhaps due to soil erosion or dust transport from neighbouring desert regions (Fig. 15). Prasad et al. (2007) reported similar AE values during April–June over the IGP region and AE <0.2 for a high dust event. The wavelength-dependence of the absorption of mineral dust depends on its composition, primarily hematite and certain clays. The AAE of Saharan dust particles was in the range of 1–2 (Collaud Coen et al., 2004). The results of this study show few data points with AE<0.2 and AAE >1, indicating that occasionally IGP has regionally influenced dust transport. The high occurrence of AE >1 and AAE >1 values suggests that the IGP region is mainly influenced by urban and biomass sources (Fig. 15).

5.3 Regional scale atmospheric radiative forcing

The Indian Ocean Experiment (INDOEX) documented for the first time (Ramanathan et al., 2001a) the haze-induced reduction in surface solar radiation and large atmospheric absorption at the regional scale and its importance in the hydrological cycle. Regionally, the absorbing haze reduced surface solar radiation by an amount comparable to 50 % of the total ocean heat flux, and nearly doubled the lower tropospheric solar heat-

ACPD
11, 21319–21361, 2011

ing (Ramanathan et al., 2001) over the Indian Ocean during December to April. The haze-induced reduction in surface solar radiation (surface forcing at $-23\,W\,m^{-2}$) is 3 times as large as the reflected solar radiation at TOA (TOA forcing at $-7\,W\,m^{-2}$) for clear skies and a consequence of large atmospheric absorption (Ramanathan et al., 2001). However, the haze over the Indian Ocean is a layer of pollutants and particles from natural and anthropogenic sources that are transported from nearby continental land regions. To quantify haze influence on regional and local climate, several observational studies were conducted over mainland regions. One such observation is a seasonal and diurnal average reduction in surface solar radiation observed about $32\pm5\,W\,m^{-2}$ over the IGB, using data collected over Kathmandu, Nepal, for a three-year mean (2001–2003) in the months of October to May (Ramanathan and Ramana, 2005).

To quantify clear sky atmospheric aerosol radiative forcing in the IGP region, cloud-screened monthly mean Kanpur AERONET measured spectral AOD, spectral SSA, column water vapor, ozone, monthly CALIPSO extinction profiles and solar zenith angle were used as inputs to the Monte Carlo Aerosol Cloud Radiation (MACR) model. The MACR is a photon transport radiative transfer algorithm described by Podgorny et al. (2000). Several case studies have proven that MACR calculations had a good agreement with observations (Ramanathan et al., 2001a, 2007; Ramana and Ramanathan, 2006). The observed monthly mean of 674 nm AOD was in the range of 0.35–0.65, with a maximum of ~0.65 being observed in April and May 2010 and a minimum of ~0.35 observed in March 2010 (Fig. 16). The SSA was observed at a minimum of ~0.83 at 674 nm in April 2010 (Fig. 16). Calculated clear sky atmospheric aerosol forcing efficiencies were between $+41\,W\,m^{-2}$ and $+66\,W\,m^{-2}$, SSA at 0.92 to 0.83 at 670 nm wavelength, respectively (Fig. 16). Maximum forcing efficiencies were observed in April. Clear-sky atmospheric aerosol forcing was in the range of $+22\,W\,m^{-2}$ to $+42\,W\,m^{-2}$ with a mean of $+29\,W\,m^{-2}$ (Fig. 16). The present study estimated atmospheric aerosol forcing values are within the range of reported values for the IGP region by Dey and Tripathi (2008) and Ramana et al., (2004).

ACPD
11, 21319–21361, 2011

6 Conclusions

Most of the earlier BC studies in the region dealt with the urban environment and do not accurately represent the rural emission scenario. The present study reports on ambient aerosol optical characteristics in rural IGP locations. The ambient BC concentration at the Project Surya village was observed in the range of 3.2–56 $\mu g\,m^{-3}$. The BC concentration reached the maximum during the winter, and gradually decreased towards the pre-monsoon period. Rural BC concentrations were well within the limits of observed urban BC, suggesting that rural emissions play as significant role as urban emissions in regional climate. The ambient BC diurnal variation based on cooking patterns indicates that BC emissions from cook stoves are a major source of ambient BC. This is further validated by Rehman et al. (2011) from aerosol absorption properties and EC/OC fraction. The observed Angstrom exponent of the absorption coefficient (AAE) for SVI_1 was greater than 1.6 in all four seasons, suggesting a significant biomass contribution. The SSA was observed in the range 0.7–0.9 at the surface, which indicates a highly absorbing aerosol. The estimated mean aerosol atmospheric forcing was observed at 29 $W\,m^{-2}$. Local to regional scale column optical properties were found to be well correlated, indicating that emission contributions from biomass and fossil fuel have similar influence in the whole region.

Acknowledgements. The authors wish to acknowledge private donors (E. Frieman, and D. Zaelke), the National Science Foundation (Grant AGS-1016496), the Swedish International Development Agency (through the United Nations Environment Programme, UNEP), The Vetlesen and the Alderson Foundations (through the Scripps Institution of Oceanography) for funding Project Surya. The authors thank UNEP for sponsoring Project Surya. Special thanks are extended to all individuals and organizations that have provided the data used in this study. The CALIPSO data were obtained via the NASA Langley Research Center website (http://www-calipso.larc.nasa.gov/). The MODIS data were obtained via the NASA Goddard Space Flight Center website (http://modis.gsfc.nasa.gov/). The authors also thank AERONET staff and data collection, calibration and processing. AERONET data was obtained via NASA AERONET website (http://aeronet.gsfc.nasa.gov/new_web/index.html).

ACPD
11, 21319–21361, 2011

References

Anderson, T. L. and Ogren, J. A.: Determining aerosol radiative properties using the TSI 3563 integrating nephelometer, Aerosol Sci. Technol., 29, 57–69, 1998.

Andreae, M. O. and Gelencser, A.: Black carbon or brown carbon? The nature of light-absorbing carbonaceous aerosols, Atmos. Chem. Phys., 6, 3131–3148, doi:10.5194/acp-6-3131-2006, 2006.

Arnott, W., Hamasha, K., Moosmüller, H., Sheridan, P. J., and Ogren, J. A.: Towards aerosol light-absorption measurements with a 7-wavelength aethalometer: Evaluation with a photoacoustic instrument and 3-wavelength nephelometer, Aerosol Sci. Technol., 39(1), 17–29, 2005.

Babu, S. S. and Moorthy, K. K.: Aerosol black carbon over tropical coastal station in India, Geophys. Res. Lett., 29(23), 2098, doi:10.1029/2002GL015662, 2002.

Beegum, G. N., Moorthy, K. K., Babu, S. S., Sathhesh, S., Vinoj, V., Badarinath, K., Safai, P., Devara, P., Singh, S., Vinod, Dumka, U., and Pant, P.: Spatial distribution of aerosol black carbon over India during pre-monsoon season, Atmos. Environ., 43, 1071–1078, 2009.

Bergstrom, R.W., Pilewskie, P., Russell, P. B., Redemann, J., Bond, T. C., Quinn, P. K., and Sierau, B.: Spectral absorption properties of atmospheric aerosols, Atmos. Chem. Phys., 7, 5937–5943, doi:10.5194/acp-7-5937-2007, 2007.

Chung, C. E., Ramanathan, V., Carmichael, G., Kulkarni, S., Tang, Y., Adhikary, B., Leung, L. R., and Qian, Y.: Anthropogenic aerosol radiative forcing in Asia derived from regional models with atmospheric and aerosol data assimilation, Atmos. Chem. Phys., 10, 6007–6024, doi:10.5194/acp-10-6007-2010, 2010.

Collaud Coen, M., Weingartner, E., Schaub, D., Hueglin, C., Corrigan, C., Henning, S., Schikowski, M., and Baltensperger, U.: Saharan dust events at the Jungfraujoch: Detection by wavelength dependence of the single scattering albedo and first climatology analysis, Atmos. Chem. Phys., 4, 2465–2480, doi:10.5194/acp-4-2465-2004, 2004.

Corrigan C. E., Ramanathan, V., and Schauer, J. J.: Impact of monsoon transitions on the physical and optical properties of aerosols, J. Geophys. Res., 111, D18208, doi:10.1029/2005JD006370, 2006.

Dey, S. and Tripathi, S. N.: Aerosol direct radiative effects over Kanpur in the Indo-Gangetic basin, northern India: Long-term (2001–2005) observations and implications to regional climate, J. Geophys. Res., 113, D04212, doi:10.1029/2007JD009029, 2008.

ACPD
11, 21319–21361, 2011

Dubovik, O., Holben, B., Eck, T. F., Smirnov, A., Kaufman, Y. J., King, M. D., Tanré, D., and Slutsker, I.: Variability of absorption and optical properties of key aerosol types observed in worldwide locations, J. Atmos. Sci., 59, 590–608, 2002.

Flanner, M., Zender, C. S., Hess, P., Mahowald, N., Painter, T., Ramanathan, V., and Rasch, P.: Springtime warming and reduced snow cover from carbonaceous particles, Atmos. Chem. Phys, 9, 2481–2497, doi:10.5194/acp-9-2481-2009, 2009.

Gadhavi, H. and Jayaraman, A.: Absorbing aerosols: contribution of biomass burning and implications for radiative forcing, Ann. Geophys., 28, 103–111, doi:10.5194/acp-28-103-2010, 2010.

Ganguly, D., Ginoux, P., Ramaswamy, V., Winker, D. M., Holben, B. N., and Tripathi, S. N.: Retrieving the composition and concentration of aerosols over the Indo-Gangetic basin using CALIOP and AERONET data, Geophys. Res. Lett., 36, L13806, doi:10.1029/2009GL038315, 2009.

Ganguly, D., Jayaraman, A., Rajesh, T. A., and Gadhavi, H.: Wintertime aerosol properties during foggy and non-foggy days over urban center Delhi and their implications for shortwave radiative forcing, J. Geophys. Res. 111, D15217, doi:10.1029/2005JD007029, 2006.

Hyvärinen, A.-P., Lihavainen, H., Komppula, M., Sharma, V. P., Kerminen, V.-M., Panwar, T. S., and Viisanen, Y.: Continuous measurements of optical properties of atmospheric aerosols in Mukteshwar, Northern India, J. Geophys. Res., 114, D08207, doi:10.1029/2008JD011489, 2009.

Jacobson, M. Z.: Short-term effects of controlling fossil-fuel soot, biofuel soot and gases, and methane on climate, arctic ice, and air pollution health, J. Geophys. Res., 115, D14209, doi:10.1029/2009JD013795, 2010.

Kar, A., Praveen, P. S., Suresh, R., Rehman, I. H., Singh, L., Singh, V. K., Ahmed, T., Burney, J., and Ramanathan, V..: Real time assessment of black carbon pollution in rural households due to cooking in traditional and improved biomass stoves, prepared for Submission to Environ. Sci. Technol., 2011.

Kirchstetter, T. W., Novakov, T., and Hobbs, P. V.: Evidence that the spectral dependence of light absorption by aerosols is affected by organic carbon, J. Geophys. Res., 109, D21208, doi:10.1029/2004JD004999, 2004.

Krishnan, R. and Ramanathan, V.: Evidence of surface cooling from absorbing aerosols, Geophys. Res. Lett., 29, 1340, doi:10.1029/2002GL014687, 2002.

Latha, K. M. and Badarinath, K. V. S.: Seasonal variations of black carbon aerosols and total

ACPD
11, 21319–21361, 2011

aerosol mass concentrations over urban environment in India, Atmos. Environ., 39, 4129–4141, 2005.
Lau, K. M., Ramanathan, V., Wu, G. X., Li, Z., Tsay, S. C., Hsu, C., Sikka, R., Holben, B., Lu, D., Tartari, G., Chin, M., Koudelova, P., Chen, H., Ma, Y., Huang, J., Taniguchi K., and Zhang, R.: The Joint Aerosol-Monsoon Experiment, B. Am. Meteorol. Soc., 89, 1–15, 2008.
Lyamani, H., Olmo, F. J., and Alados-Arboledas, L.: Physical and optical properties of aerosols over an urban location in Spain: seasonal and diurnal variability, Atmos. Chem. Phys., 10, 239–254, doi:10.5194/acp-10-239-2010, 2010.
Marinoni, A., Cristofanelli, P., Laj, P., Duchi, R., Calzolari, F., Decesari, S., Sellegri, K., Vuillermoz, E., Verza, G. P., Villani, P., and Bonasoni, P.: Aerosol mass and black carbon concentrations, a two year record at NCO-P (5079 m, Southern Himalayas), Atmos. Chem. Phys., 10, 8551–8562, doi:10.5194/acp-10-8551-2010, 2010.
Menon, S., Hansen, J., Nazarenko, L., and Luo, Y.: Climate effects of black carbon aerosols in China and India, Science, 297, 2250–2253, 2002.
Menon, S., Koch, D., Beig, G., Sahu, S., Fasullo, J., and Orlikowski, D.: Black carbon aerosols and the third polar ice cap, Atmos. Chem. Phys., 10, 4559–4571, doi:10.5194/acp-10-4559-2010, 2010.
Molina, M., Zaelke, D., Sarma, K. M., Andersen, S. O., Ramanathan, V., and Kaniaru, D.: Reducing abrupt climate change risk using the Montreal Protocol and other regulatory actions to complement cuts in CO_2 emissions, Proc. Natl. Acad. Sci., 106(49), 20616–20621, doi/10.1073/pnas.0902568106, 2009.
Müller, T., Nowak, A., Wiedensohler, A., Sheridan, P., Laborde, M., Covert, D. S., Marinoni, A., Imre, K., Henzing, B., Roger, J.-C., Martins dos Santos, S., Wilhelm, R., Wang, Y.-Q., and de Leeuw, G.: Angular illumination and truncation of three different integrating nephelometers: implications for empirical, size-based corrections, Aerosol Sci. Technol., 43(6), 581–586, 2009.
Nair, V. S., Moorthy, K. K., Alappattu, D. P., Kunhikrishnan, P. K., George, S., Nair, P. R., Babu, S. S, Abish, B., Satheesh, S. K., Tripathi, S. N., Niranjan, K., Madhavan, B. L., Srikant, V., Dutt, C. B. S., Badarinath, K. V. S., and Reddy, R. R.: Wintertime aerosol characteristics over the Indo-Gangetic Plain (IGP): Impacts of local boundary layer processes and long-range transport, J. Geophys. Res., 112, D13205, doi:10.1029/2006JD008099, 2007.
Pan, X. L., Yan, P., Tang, J., Ma, J. Z., Wang, Z. F., Gbaguidi, A., and Sun, Y. L.: Observational study of influence of aerosol hygroscopic growth on scattering coefficient over rural area near

ACPD
11, 21319–21361, 2011

Beijing mega-city, Atmos. Chem. Phys., 9, 7519–7530, doi:10.5194/acp-9-7519-2009, 2009.
Pettus, A.: Agricultural Fires and Arctic Climate Change, Clean Air Task Force, May, 2009.
Podgorny, I. A., Conant, W., Ramanathan, V., and Satheesh, S. K.: Aerosol modulation of atmospheric and surface solar heating over the tropical indian ocean, Tellus, 52B, 947–958, 2000.
Prasad, A. K., Singh, S., Chauhan, S. S., Srivastava, M. K., Singh, R. P., and Singh, R.: Aerosol radiative forcing over the Indo-Gangetic plains during major dust storms, Atmos. Environ., 41, 6289–6301, doi:10.1016/j.atmosenv.2007.03.060, 2007.
Ram, K. and Sarin, M. M.: absorption coefficient and site-specific mass absorption efficiency of elemental carbon in aerosols over urban, rural, and high-altitude sites in India, Environ. Sci. Technol. 43, 8233–8239, 2009.
Ram, K., Sarin, M. M., and Hegde, P.: Long-term record of aerosol optical properties and chemical composition from a high-altitude site (Manora Peak) in Central Himalaya, Atmos. Chem. Phys., 10, 11791–11803, doi:10.5194/acp-10-11791-2010, 2010.
Ramachandran, S. and Kedia, S.: Black carbon aerosols over an urban region: Radiative forcing and climate impact, J. Geophys. Res., 115, D10202, doi:10.1029/2009JD013560, 2010.
Ramana, M. V. and Ramanathan, V.: Abrupt transition from natural to anthropogenic aerosol radiative forcing: Observations at the ABC-Maldives Climate Observatory, J. Geophys. Res., 111, D20207, doi:10.1029/2006JD007063, 2006.
Ramana, M. V., Ramanathan, V., Podgorny, I. A., Pradhan, B. B., and Shrestha, B.: The direct observations of large aerosol radiative forcing in the Himalayan Region, Geophy. Res. Lett., 31, L05111, doi:10.1029/2003GL018824, 2004.
Ramanathan, V. and Balakrishnan, K.: Project Surya: Reduction of air pollution and global warming by cooking with renewable sources, White paper, available at online: http://www.projectsurya.org/storage/Surya-WhitePaper.pdf, 2007.
Ramanathan, V. and Carmichael, G.: Global and regional climate changes due to black carbon, Nat. Geosci., 1, 221–227, 2008.
Ramanathan, V., Crutzen, P. J. , Lelieveld, J., Mitra, A. P., Althausen, D., Anderson, J., Andreae, M. O., Cantrell, W., Cass, G. R., Chung, C. E., Clarke, A. D., Coakley, J. A., Collins, W. D., Conant, W. C., Dulac, F., Heintzenberg, J., Heymsfield, A. J., Holben, B., Howell, S., Hudson, J., Jayaraman, A., Kiehl, J. T., Krishnamurti, T. N., Lubin, D., McFarquhar, G., Novakov, T., Ogren, J. A., Podgorny, I. A., Prather, K., Priestley, K., Prospero, J. M., Quinn, P. K.,

ACPD
11, 21319–21361, 2011

Rajeev, K., Rasch, P., Rupert, S., Sadourny, R., Satheesh, S. K., Shaw, G. E., Sheridan, P., and Valero, F. P. J.: The Indian Ocean Experiment: An integrated analysis of the climate forcing and effects of the Great Indo-Asian Haze, J. Geophys. Res., 106(D22), 28371–28398, 2001a.

Ramanathan, V., Crutzen, P. J., Kiehl, J. T., and Rosenfeld, D.: Aerosols, Climate, and the Hydrological Cycle, Science, 294, 2119–2124, 2001b.

Ramanathan, N., Lukac, M., Ahmed, T., Kar, A., Siva, P., Honles, T., Leong, I., Rehman, I.H., Schauer, J., and Ramanathan, V.: A cellphone based system for global monitoring of black carbon, Atmos. Environ., 45, 4481–4487, 2011.

Ramanathan, V. and Ramana, M. V.: Persistent, widespread, and strongly absorbing haze over the Himalayan foothills and the Indo-Gangetic Plains, Pure Appl. Geophys., 162, 1609–1626, 2005.

Ramanathan V., Ramana, M. V., Roberts, G., Kim, D., Corrigan, C. E., Chung, C. E., and Winker, D.: Warming trends in Asia amplified by brown cloud solar absorption, Nature, 448, 575–578, doi:10.1038/nature06019, 2007.

Ramanathan, V. and Wallack, J.: The other climate changes, why black carbon also matters, For. Affairs, Sep/Oct 2009, 105–113, 2009.

Ramanathan, V. and Xu, Y.: The Copenhagen Accord for limiting global warming: Criteria, constraints, and available avenues, Proc. Natl. Acad. Sci., 107(18) 8055–8062, 2010.

Reddy, M. S. and Boucher, O.: Climate impact of black carbon emitted from energy consumption in the world's regions, Geophys. Res. Lett., 34, L11802, doi:10.1029/2006GL028904, 2007.

Rehman, I. H., Ahmed, T., Praveen, P. S., Kar, A., and Ramanathan, V.: Black carbon emissions from biomass and fossil fuels 1 in rural India, Atmos. Chem. Phys., 11, 7289–7299, doi:10.5194/acp-11-7289-2011, 2011.

Russell, P. B., Bergstrom, R. W., Shinozuka, Y., Clarke, A. D., De- Carlo, P. F., Jimenez, J. L., Livingston, J. M., Redemann, J., Dubovik, O., and Strawa, A.: Absorption Angstrom Exponent in AERONET and related data as an indicator of aerosol composition, Atmos. Chem. Phys., 10, 1155–1169, doi:10.5194/acp-10-1155-2010, 2010.

Safai, P. D., Kewat, S., Praveen, P. S., Rao, P. S. P., Momin, G. A., Ali, K., and Devara, P. C. S.: Seasonal Variation of black carbon aerosol over tropical urban city of Pune,India, Atmos. Environ., 41, 2699–2709, 2007.

Safai, P. D., Kewat, S., Pandithurai, G., Praveen, P. S., Ali, K., Tiwari, S., Rao, P. S. P., Bud-

ACPD
11, 21319–21361, 2011

hawant, K. B., Saha, S. K., and Devara, P. C. S.: Aerosol characteristics during winter fog at Agra, North India, J. Atmos. Chem., 61, 101–118, 2008.

Sauvain, J. J., Vu Duc, T., and Guillemin, M.: Exposure to polycyclic aromatic compounds and health risk assessment for diesel exposed workers, Int Arch. Occup. Environ. Health., 76, 443–455, 2003.

Schauer, J. J., Mader, B. T., DeMinter, J. T., Heidemann, G., Bae, M. S., Seinfeld, J. H., Flagan, R, C., Cary, R. A., Smith, D., Huebert, B. J., Bertram, T., Howell, S., Kline, J. T., Quinn, P., Bates, T., Turpin, B., Lim, H. J., Yu, J. Z., Yang, H., and Keywood, M. D.: ACE-Asia intercomparison of a thermal-optical method for the determination of particle-phase organic and elemental carbon, Environ. Sci. Technol., 37, 993–1001, 2003.

Schmid, O., Artaxo, P., Arnott, W. P., Chand, D., Gatti, L. V., Frank, G. P., Hoffer, A., Schnaiter, M., and Andreae, M. O.: Spectral light absorption by ambient aerosols influenced by biomass 15 burning in the Amazon Basin. I: Comparison and field calibration of absorption measurement techniques, Atmos. Chem. Phys., 6, 3443–3462, doi:10.5194/acp-6-3443-2006, 2006.

Schwarz, J.: Measurement of the mixing state, mass, and optical size of individual black carbon particles in urban and biomass burning emissions. Geophys. Res. Lett., 35, L13810, doi:10.1029/2008GL033968, 2008.

Schwarze, P. E., Ovrevik, J., and Lag, M.: Particulate matter properties and health effects: consistency of epidemiological and toxicological studies, Human Exp. Toxicol., 25, 559–579, 2006.

Smith, K. R., Mehta, S., and Feuz, M.: Indoor air pollution from household use of solid fuels, in: Comparative quantification of health risks: global and regional burden of disease attributable to selected major risk factors, edited by: Ezzati M., Geneva, World Health Organization, 2004.

Sreekanth, V., Niranjan, K., and Madhavan, B. L.: Radiative forcing of black carbon over eastern India, Geophys. Res. Lett., 34, L17818, doi:10.1029/2007GL030377, 2007.

Stone, E. A., Schauer, J. J., Pradhan, B. B., Dangol, P. M., Habib, G., Venkataraman, C., and Ramanathan, V.: Characterization of emissions from South Asian biofuels and application to source apportionment of carbonaceous aerosol in the Himalayas, J. Geophys. Res., 115, D06301, doi:10.1029/2009JD011881, 2010.

Tripathi, S. N., Dey, S., Tare, V., and Satheesh, S. K.: Aerosol black carbon radiative forcing at an industrial city in northern India, Geophys. Res. Lett., 32, L08802, doi:10.1029/2005GL022515, 2005.

ACPD

11, 21319–21361, 2011

Venkataraman, C., Habib, G., Eiguren-Fernandez, A., Miguel, A. H., and Friedlander, S. K.: Residential biofuels in South Asia: carbonaceous aerosol emissions and climate impacts, Science, 307, 1454–1456, 2005.

Venkataraman, C., Habib, G., Kadamba, D., Shrivastava, M., Leon, J.-F., Crouzille, B., Boucher, O., and Streets, D. G.: Emissions from open biomass burning in India: integrating the inventory approach with higher solution Moderate Resolution Imaging Spectroradiometer (MODIS) active fire and land count data, Global Biogeochem. Cy., 20, GB2013, doi:10.1029/2005GB002547, 2006.

Yan, P., Tang, J., Huang, J., Mao, J. T., Zhou, X.J., Liu, Q., Wang, Z. F., and Zhou, H. G.: The measurement of aerosol optical properties at a rural site in Northern China, Atmos. Chem. Phys., 8, 2229–2242, doi:10.5194/acp-8-2249-2008, 2008.

ACPD

11, 21319–21361, 2011

Table 1. Comparison of SVI_1 BC concentration ($\mu g\,m^{-3}$) with earlier reported BC concentration ($\mu g\,m^{-3}$) at different locations in India.

Location	Site	Winter	Pre-Monsoon	Monsoon	Post-Monsoon	Year	Reference
SVI_1	Rural, IGP	16.3	12.7	3.8	13.8	2009–2010	Present
Gadanki	Rural		4	1		2008	Gadhavi and Jayaraman (2010)
Nepal, Godavari	Rural	2.3–0.8	1.7–1.1	0.2–0.5	0.5–0.5	2006	Stone et al. (2010)
Kharagpur	Urban, IGP	9.3–7.5	6.9–2.7			2006	Beegum et al. (2009)
Kanpur	Urban, IGP	6–20				2004	Tripati et al. (2005)
Agra	Urban, IGP	17.4–10.5				2004	Safai et al. (2008)
Delhi	Urban, IGP	27–19	12–8.1			2006	Beegum et al. (2009)
Ahmedabad	Urban	11.6	3.9	2.1	10.9	2008	Ramachandran and Kedia (2010)
Pune	Urban	7.4	3.3	1.3	6	2005	Safai et al. (2007)
Hyderabad	Urban	21–25	12–15			2006	Beegum et al. (2009)
Trivandrum,	Urban, Costal	~5		~1.5		2000–2001	Babu and Moorthy (2002)
Vishakhapatnam	Urban, Costal	8	3.3	1.7	0.4	2005–2006	Sreekanth et al. (2007)
Manora Peak	Hill station	1.8	0.9	0.5	1.4	2005–2008	Ram et al. (2010)
Mukteshwar	Hill station	1.2–0.5	1.4–0.9	0.8–0.3	0.8–0.7	2005–2007	Hyvärinen et al. (2009)
Nepal, NCOP	Hill station	0.13	0.3	0.06	0.14	2006–2007	Marinoni et al. (2010)
Port Blair	Marine	2.6	1.8–1.3			2006	Beegum et al. (2009)
MCOH, Maldives	Marine	0.7		0.04		2004–2005	Corrigen et al. (2006)
Minicoy	Marine	0.5	0.2–0.07			2006	Beegum et al. (2009)

ACPD
11, 21319–21361, 2011

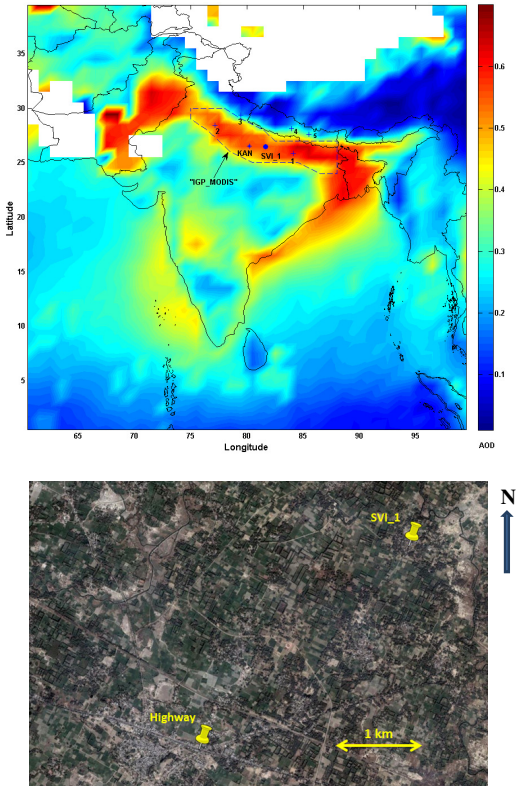

Fig. 1. (Top) MODIS TERRA mean aerosol optical depth (AOD) for the period 1 October 2009 to 14 April 2010 over India. SVI_1 (Surya village) represents our sampling location. KAN represents neighbouring urban (130 km away from SVI_1) AERONET site at Kanpur (26.30′ N, 80.31′ E). Other AERONET sites in the IGP region are shown as 1 (Gandhi College; 25.52′ N, 84.07′ E), 2 (Gual Pahari; 28.25′ N, 77.09′ E) and 3 (Nainital; 29.21′ N, 79.27′ E) located in India; 4 (Pokhara; 28.09′ N, 83.58′ E) and 5 (Kathmandu University; 27.36′ N, 85.32′ E) located in Nepal. Dashed line represents the "IGP_MODIS" region used for calculating regional mean AOD (using MODIS). (Bottom) Satellite view showing locations of our two sampling sites; SVI_1 and highway.

ACPD
11, 21319–21361, 2011

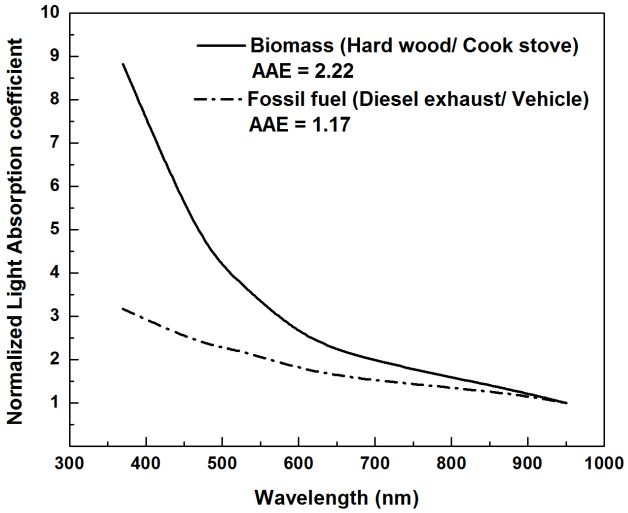

Fig. 2. Normalized light absorption coefficient of aerosol samples from biomass (hard wood in traditional mud cook stove) and fossil fuel (diesel) combustion measured using Aethalometer AE31. AAE represents the absorption angstrom exponent.

ACPD
11, 21319–21361, 2011

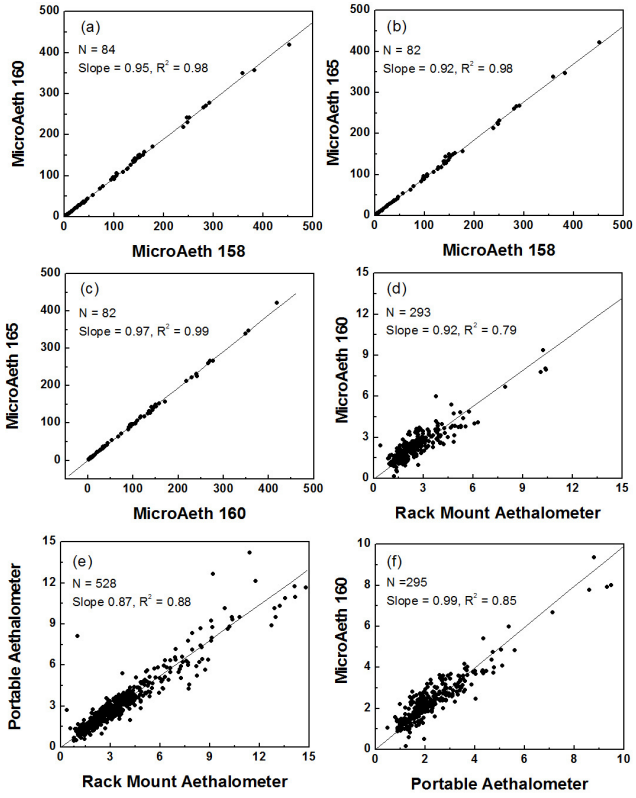

Fig. 3. Inter-comparison of BC measurements between three different models of Aethalometers (microAeth, Rack Mount and Portable) used in our study.

ACPD
11, 21319–21361, 2011

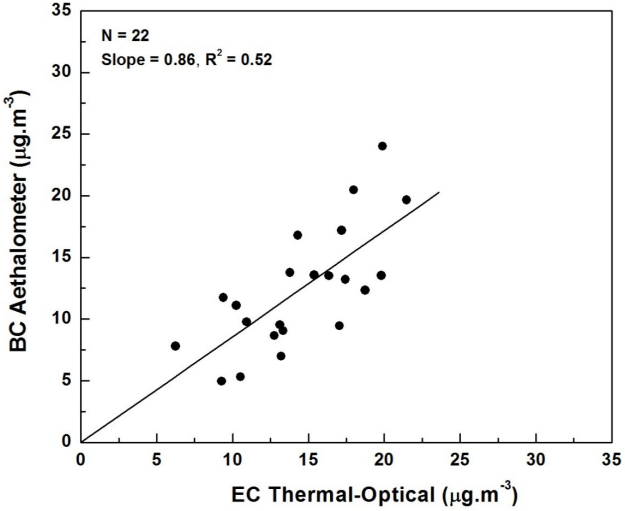

Fig. 4. Comparison of BC measurements (from Aethelometer AE31) and EC measurements (from thermal-optical analyzer) at village center (VC) located in Surya Village (SVI_1).

ACPD
11, 21319–21361, 2011

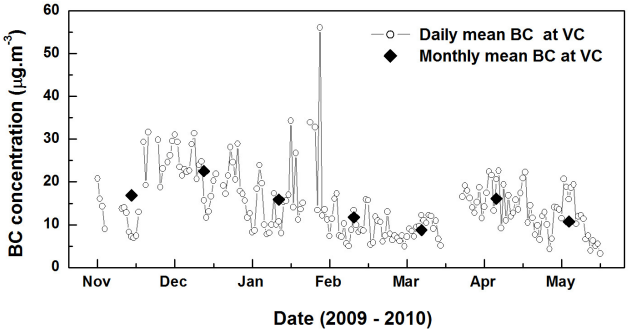

Fig. 5. Daily and monthly mean variation of BC concentrations at SVI_1 village centre (VC).

ACPD
11, 21319–21361, 2011

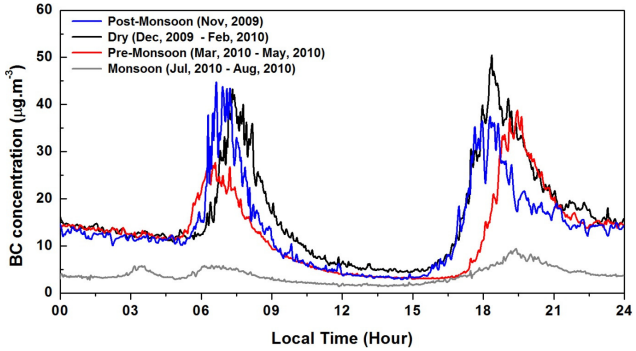

Fig. 6. Diurnal variation of seasonal mean BC concentration at SVI_1 village centre (VC).

ACPD
11, 21319–21361, 2011

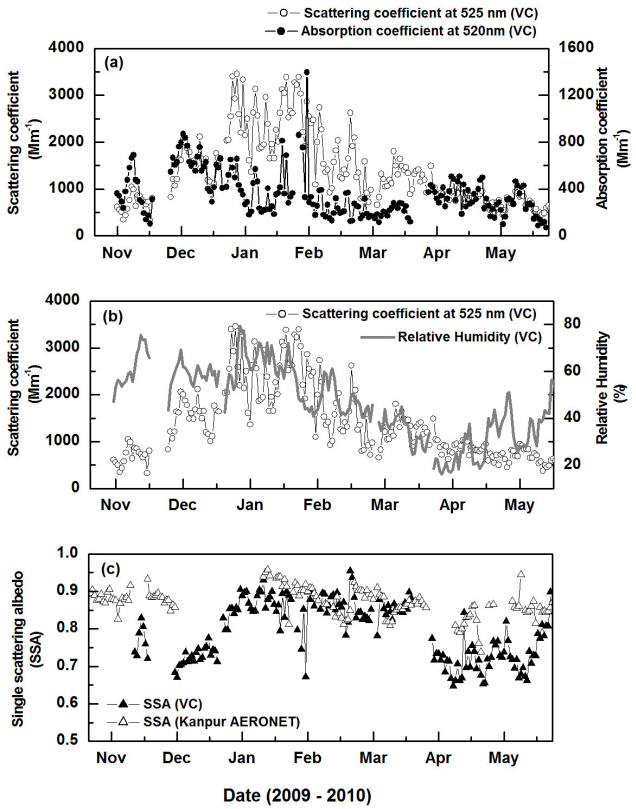

Fig. 7. **(a)** Daily variation of aerosol absorption coefficient and scattering coefficient from surface observation at SVI_1 village center (VC), **(b)** Daily variation of scattering coefficient and relative humidity (RH) from surface observation at SVI_1 village center (VC). **(c)** Comparison of surface SSA at VC with the column measured SSA from AERONET site located in neighbouring urban centre, Kanpur.

ACPD
11, 21319–21361, 2011

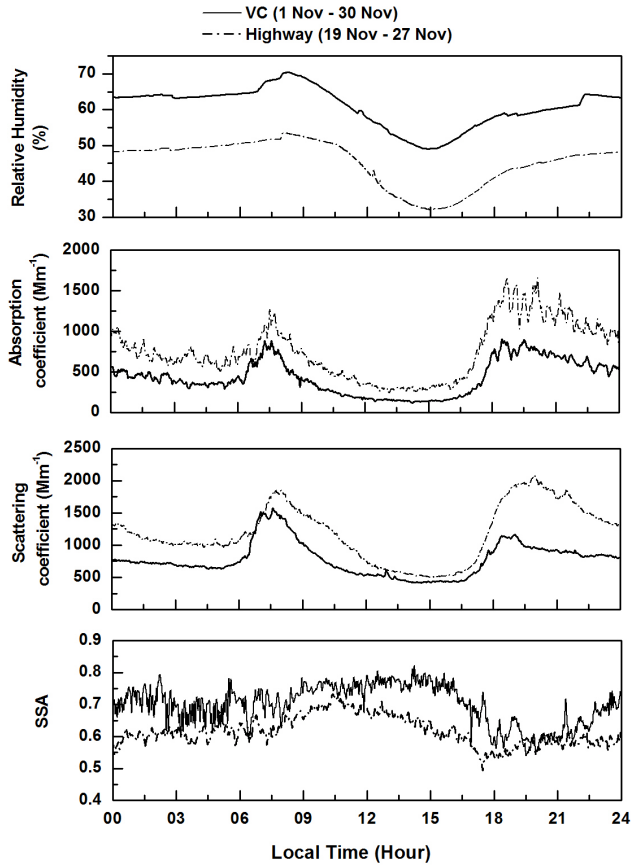

Fig. 8. Comparison of diurnal variation of relative humidity, absorption coefficient, scattering coefficient and single scattering albedo (SSA) at SVI_1 village center (VC) and highway (traffic junction).

ACPD
11, 21319–21361, 2011

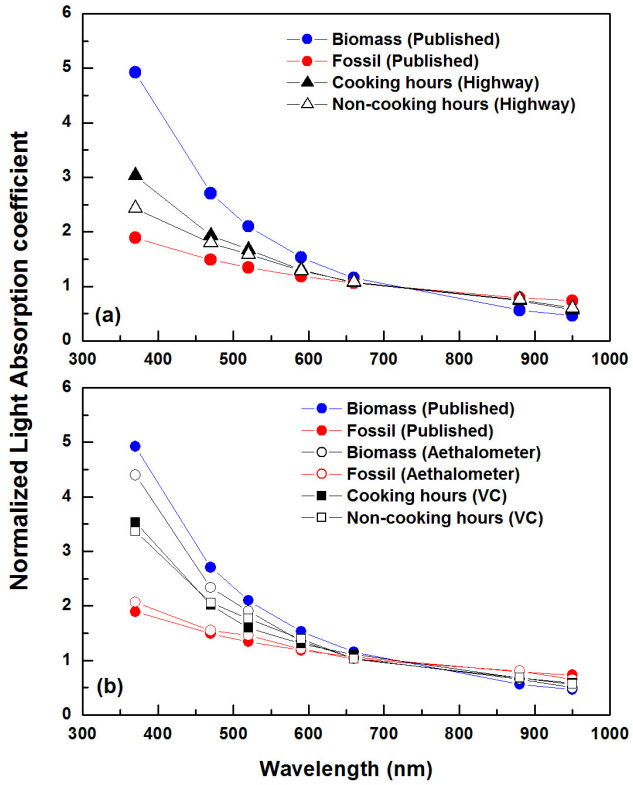

Fig. 9. Comparison of normalized light absorption coefficient of aerosol during cooking and non-cooking hours at **(a)** Highway and **(b)** SVI_1 village center (VC). Also show is earlier published (Kirchstetter et al., 2004) and the observed Aethalometer response to biomass and fossil fuel combustion aerosols.

ACPD
11, 21319–21361, 2011

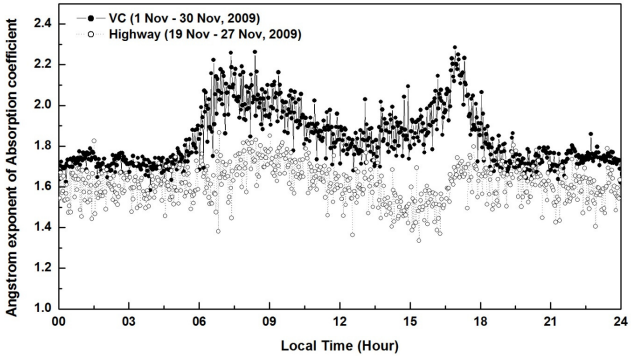

Fig. 10. Diurnal variation of Angstrom exponent of absorption coefficient at village center (VC) and highway.

ACPD
11, 21319–21361, 2011

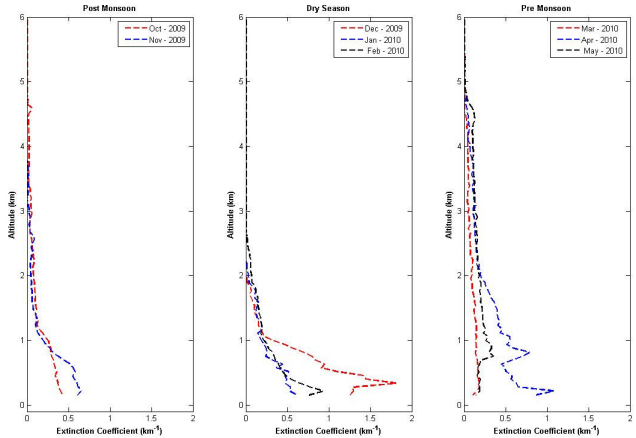

Fig. 11. Monthly mean LIDAR extinction profiles (532 nm) from CALIPSO for the grid (26–27° N and 80–82° E) for post-monsoon, dry and pre-monsoon seasons, respectively. SVI_1 is located within this grid.

ACPD
11, 21319–21361, 2011

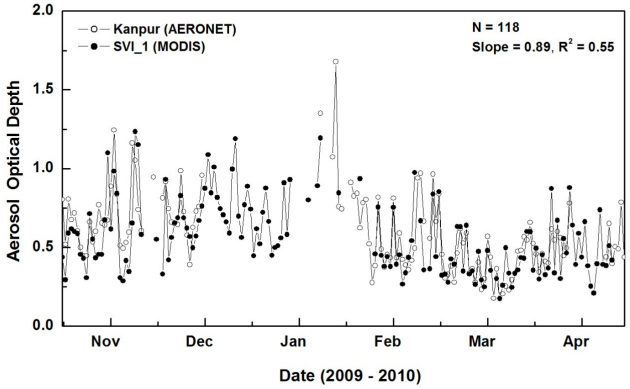

Fig. 12. Comparison of temporal variation of daily mean MODIS aerosol optical depth (AOD) at Surya Village (SVI_1) and AERONET measured column AOD at neighbouring urban centre (130 km away from SVI_1), Kanpur.

ACPD
11, 21319–21361, 2011

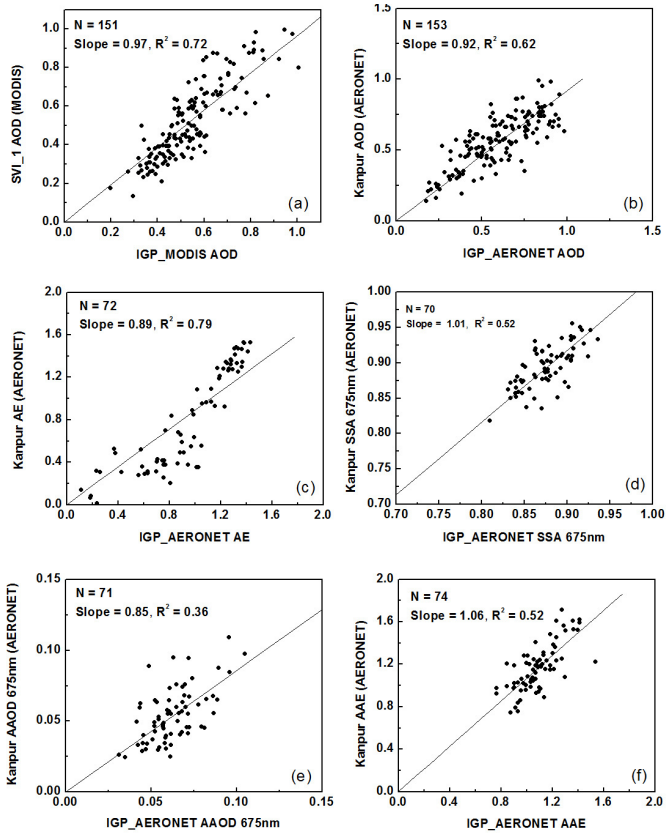

Fig. 13. Comparison of daily mean IGP_MODIS and IGP_AERONET to local (Kanpur and SVI_1) scale aerosol optical properties for the period November 2009 to May2010. AOD represents aerosol optical depth , AAOD represents absorption aerosol optical depth, SSA represents single scattering albedo, AE represents Angstrom exponent of AOD and AAE_C represents Angstrom exponent of AAOD. IGP_AERONET was calculated from the mean of six AERONET sites located in India and Nepal (see Fig. 1). The IGP_MODIS represents the mean of the AOD over the region shown as dashed line in Fig. 1.

ACPD
11, 21319–21361, 2011

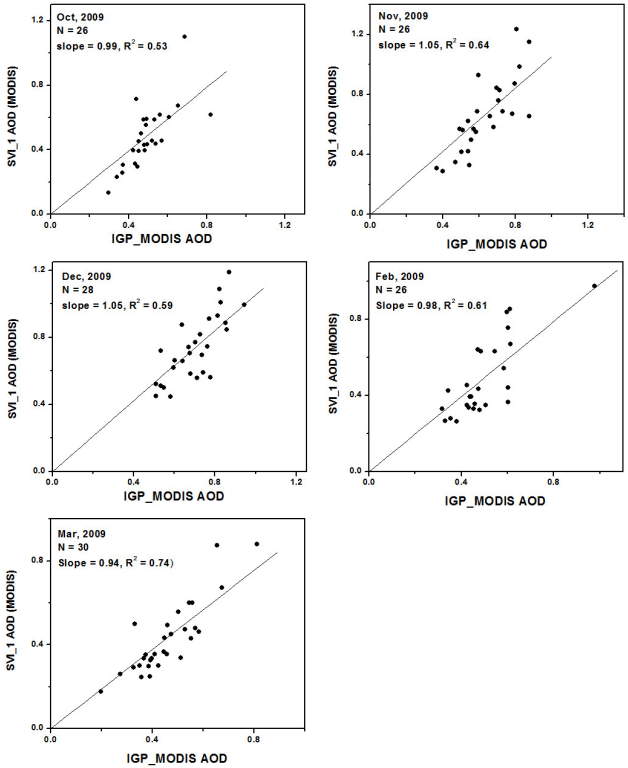

Fig. 14. Comparison of daily mean IGP_MODIS to local (SVI_1) scale MODIS aerosol optical depth (AOD) during different months. The IGP_MODIS represents the mean of the AOD over the region shown as dashed line in Fig. 1.

ACPD
11, 21319–21361, 2011

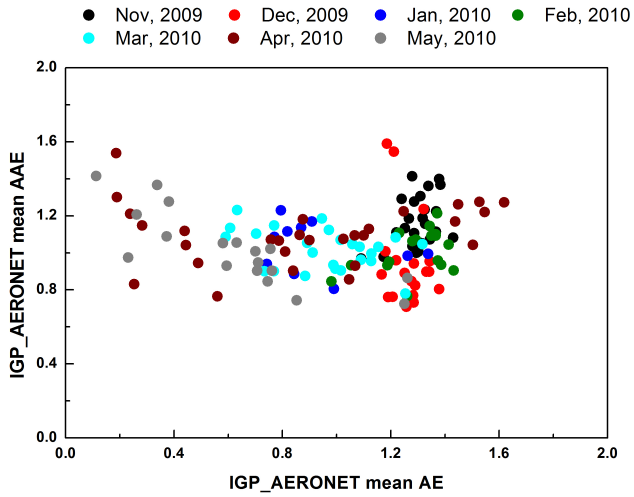

Fig. 15. Scatter plot of IGP_AERONET daily mean Angstrom exponent of AOD (AE) and daily mean Angstrom exponent of AAOD (AAE) for the IGP region. IGP_AERONET was calculated from the mean of six AERONET sites located in India and Nepal (see Fig. 1).

ACPD
11, 21319–21361, 2011

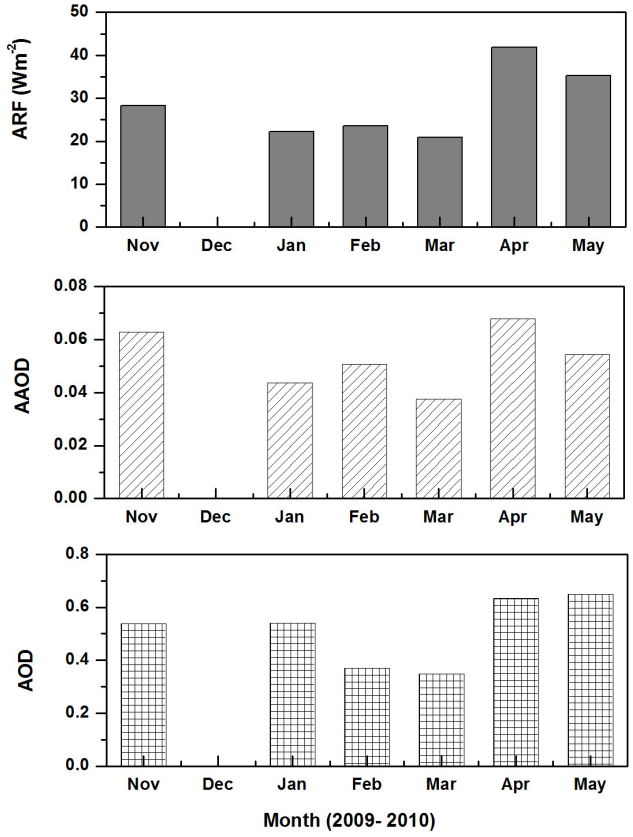

Fig. 16. Monthly mean aerosol optical depth (AOD), absorption aerosol optical depth (AAOD) and aerosol atmospheric radiative forcing (ARF) in the broadband region over Kanpur.

ACPD
11, 21319–21361, 2011